Conference on Modelling Fluid Flow (CMFF'12)
The 15th International Conference on Fluid Flow Technologies
Budapest, Hungary, September 4-7, 2012

NUMERICAL STUDY OF THE INCOMPRESSIBLE RICHTMYER-MESHKOV INSTABILITY. INTERFACE TRACKING METHODS ON GENERAL MESHES

Lluís JOFRE[1], Néstor BALCÁZAR [2], Oriol LEHMKUHL [2 3],
Jesús CASTRO [2], Assensi OLIVA [2]

[1] Corresponding Author. Heat and Mas Transfer Technological Center, Technical University of Catalonia, C/ Colom 11, 08222 Terrassa, Spain.
Tel.: (+34) 93 739 81 92, Fax: (+34) 93 739 89 20, E-mail: lluis@cttc.upc.edu
[2] Heat and Mas Transfer Technological Center, Technical University of Catalonia, C/ Colom 11, 08222 Terrassa, Spain.
Tel.: (+34) 93 739 81 92, Fax: (+34) 93 739 89 20, E-mail: cttc@cttc.upc.edu
[3] Termo Fluids S.L., Av. Jaquard 97 1-E, 08222 Terrassa, Spain.
Tel.: (+34) 93 783 61 13, E-mail: termofluids@termofluids.com

ABSTRACT

The numerical simulation of interfacial and free surface flows is a vast and interesting topic in the areas of engineering and fundamental physics, such as the study of liquid-gas interfaces, formation of droplets, bubbles and sprays, combustion problems with liquid and gas reagents, study of wave motion and others.

Many different methods for interface tracking exist, but Volume-of-Fluid and Level-Set methods are two of the most important. The Volume-of-Fluid preserves mass in a natural way but requires large computational resources. On the other hand, the Level-Set is not as accurate and mass conservative as the Volume-of-Fluid but is a faster way to track interfaces, representing them by the middle contour of a signed distance function.

The objective of this work is to analyze the advantatges and drawbacks of the Volume-of-Fluid and Level-Set methods by solving the incompressible two-liquid Richtmyer-Meshkov instability and to compare the results to experimental data.

Keywords: general mesh, interface tracking, multiphase flows, Richmyer-Meshkov instability

NOMENCLATURE

A	$[m^2]$	surface
C	$[-]$	volume fraction
$\underline{g}$	$[m/s^2]$	gravity
$\dot{m}$	$[kg/s]$	mass flux
$\underline{n}$	$[-]$	unit normal vector
p	$[Pa]$	pressure
t	$[s]$	time
$\underline{u}$	$[m/s]$	velocity vector
u	$[m/s]$	normal face velocity
V	$[m^3]$	volume
W	$[m]$	width
$\underline{x}$	$[m]$	position vector
μ	$[Pa \cdot s]$	dynamic viscosity
ρ	$[kg/m^3]$	density
$\underline{\omega}$	$[1/s]$	vorticity vector

Subscripts

c	cell
f	face
k	fluid
c_1, c_2	cells adjacent to face
P, F	nodes adjacent to face

Superscripts

CC	cell circumcenter
CG	cell center of gravity
f	face
n	discrete time level
$*$	predictor

1. INTRODUCTION

1.1. Richtmyer-Meshkov Instability

This work is focused on the study of the Richtmyer-Meshkov (RM) instability [1, 2]. Particularly, the RM instability of incompressible miscible liquids with two and three-dimensional (2D,3D) single-mode initial perturbations. The amplitude and velocity of the instability along time and vorticity is analyzed and compared to experimental data [3, 4]. The instability is solved using two different interface tracking methods: Volume-of-Fluid and Level-Set, and the momentum equation is discretizated by a staggered mesh scheme.

The RM instability occurs at a nearly planar interface separating two fluids that are impulsively accelerated in the direction normal to the interface, as a result of a impulsive body force or a passing shock wave. The initial development of the instability creates small amplitude perturbations which initially grow linearly with time. Followed by a nonlinear regime with bubbles appearing in the case of a light fluid penetrating a heavy fluid, and with spikes appearing in the case of a heavy fluid penetrating a light fluid.

The RM instabilities initiated with a single-mode 2D and 3D initial perturbations have been extensively studied and experimentally investigated beginning with the pioneering work of Richtmyer and Meshkov and lately by Niederhaus, Chapman and Jacobs. Experiments have verified the early time linear growth predicted by Richtmyer. However, no nonlinear solution capable of predicting the behavior from the early linear stages into the far nonlinear regime is available at the moment. Many researchers have developed nonlinear analyses [5], heuristic models [6] and analytical approaches [7] that capture some of the physics of the late-time asymptotic flow, but they all necessarily must incorporate empirical constants making them not general solutions.

1.2. Methods for interface tracking

The contact of different fluids or phases in motion, produces a thin region that separates them called interface. This kind of flows are named free surface or interfacial flows and are found in multiple fields such as engineering, fundamental physics, geophysics, etc. Typical examples of this phenomena are bubbles, drops, sprays, jets, waves, clouds and particularly the RM instability.

The numerical strategies used to track the motion of the interface between fluids are called interface tracking methods. There are many different methods, a general list classified in three main classes can be found in the literature by Scardovelli and Zaleski [8]. In particular, this work focuses in the Volume-of-Fluid (VOF) and Level-Set (LS) methods, since they are two of the most known and used.

The Volume-of-Fluid preserves mass in a natural way and presents no problem for reconnection or breakup of the interface but requires large computational resources. The first VOF implementations were presented in the 1970s for 2D cartesian meshes, being the method proposed by Hirt and Nichols [9] the reference one. In recent years, the method has been improved and adapted to 3D meshes, in a cartesian approach by Liovic et al. [10] and more generally to 3D cartesian and unstructured meshes by Jofre et al. [11].

On the other hand, the Level-Set is a fast way to track interfaces, representing them by the middle contour of a signed distance function, but its main drawback is the not conservation of mass. This method was first introduced in the 1980s by Osher and Sethian [12] for n-D general meshes but did not conserve mass. Recently, Olsson and Kreiss [13] have proposed a different approach for the method, based on previous works, in order to be mass conservative.

1.3. Discretizations of the Navier-Stokes equations

One of the main difficulties when solving the Navier-Stokes equations is the localization of the velocity grid points in order to avoid a checkerboard pressure field, due to the decoupling of the velocity and pressure fields present in the equations. This issue is more critical when high discontinuities are present in the domain, such as when multiphase flows or combustion problems are being solved. In order to solve this problem, there are two main mesh arrangements for the computation of the Navier-Stokes equations, the collocated and staggered schemes.

One of the first collocated schemes was presented by Rhie and Chow [14] for body-fitted meshes in the 1980s. In recent years, the scheme has been extended to unstructured meshes and improved to diminish the kinetic energy conservation error; i.g. changing the pressure gradient term by Mahesh et al. [15] and defining particular face mass fluxes that locally conserve mass by Lehmkuhl et al. [16]. The main characteristic of the scheme is that the velocity field is located at the same grid points as the pressure one, what can result in a checkerboard pressure problem when solving discontinuous flows like the RM instability.

In order to solve this problem, a staggered mesh arrangement is used in this work. This type of scheme is a numerical strategy where variables are located at different points within the mesh. Many different staggering schemes are possible. However, in this work we are interested in the scheme presented by Perot [17] since it is a generalization to unstructured meshes of the one originally presented by Harlow and Welch [18]. This scheme locates pressure at cell centers and normal velocity at cell faces. The main variable is the normal face velocity, then, velocity vectors at cell centers are interpolated from normal face velocities, in a particular form that conserves kinetic energy and momentum.

1.4. Objectives and novelty of the paper

The principal objective of this work is to demonstrate that computational fluid dynamics can be a good tool to study multiphase flows. In particular, the Richtmyer-Meshkov instability since no nonlinear solution capable of predicting the behavior at all stages has been found and the lack of generality of other heuristic models. On the other hand, it is an exigent test to check the performance of the self-developed implementations of the Volume-of-Fluid and Level-Set methods for 3D unstructured meshes, hence, allowing other more industry oriented problems to be afforded in the near future.

2. GOVERNING EQUATIONS

Interface tracking methods, such as Volume-of-Fluid and Level-Set, describe both fluids with one set of momentum equations and solve a volume fraction advection equation for the evolution of the interfaces between the two fluids.

The volume fraction color function $C_k(\underline{x})$ is defined as an identity function

$$C_k(\underline{x}) = \begin{cases} 1 & \text{if there is fluid k.} \\ 0 & \text{otherwise.} \end{cases} \quad (1)$$

Then, the discrete volume fraction of the kth fluid for a general volume is calculated as

$$C_k = \frac{\int C_k(\underline{x}) dV}{\int dV}, \quad (2)$$

it ranges from 0 to 1 and its sum over all k is unity.

If the flow is assumed to be incompressible and there is no surface tension between fluids, the volume fraction advection equation results in

$$\frac{\partial C_k}{\partial t} + \nabla \cdot (C_k \underline{u}) = 0 \quad (3)$$

and mass and momentum conservation are defined as

$$\nabla \cdot \underline{u} = 0, \quad (4)$$

$$\begin{aligned} \frac{\partial(\rho \underline{u})}{\partial t} + \nabla \cdot (\rho \underline{u}\underline{u}) = & -\nabla p \\ & + \nabla \cdot (\mu(\nabla \underline{u} + \nabla \underline{u}^T)) \\ & + \rho \underline{g}, \end{aligned} \quad (5)$$

where the fluid density and viscosity are evaluated as

$$\rho = \sum_k \rho_k C_k \quad \text{and} \quad \mu = \sum_k \mu_k C_k. \quad (6)$$

The solution of the momentum equation, Eq. (5), provides the velocity field used in the volume fraction advection equation, Eq. (3), to calculate the new volume fraction scalar field.

3. NUMERICAL MODEL

3.1. Volume fraction advection equation

The two interface tracking methods used in this work solve the volume fraction advection equation, Eq. (3), but they differ in the discretization and procedure followed to do so.

3.1.1. Volume-of-Fluid method

The VOF method discretizes the volume fraction advection equation, Eq. (3), for each cell as

$$C_k^{n+1} - C_k^n + \frac{1}{V_c} \sum_f \delta V_{k,f}^n = 0, \quad (7)$$

where the kth fluid volume flux across face f, $V_{k,f}^n$, is geometrically calculated from the total volume flux given by

$$\delta V_f = \underline{u}_f \cdot \underline{n}_f A_f \delta t = \sum_k \delta V_{k,f}. \quad (8)$$

Then, the volume fraction advection, Eq. (7), is solved for each fluid k in two steps: Interface Reconstruction and Advection. First, the interface is reconstructed by approximating its form to a geometric surface, this work reconstructs interfaces by planes using a Least Square Gradient (LSG) approach of the Youngs' method [19]. Once the interface is reconstructed, the advection step constructs volume fluxes at cell faces and cuts them by the reconstructed interface to compute the amount of fluid kth that is being fluxed through the face, this works uses a self-developed unstructured 3D unsplit advection algorithm. These two steps are explained in detail by Jofre et al. [11].

3.1.2. Level-Set method

The conservative LS method, proposed by Olsson and Kreiss [13], discretizes the volume fraction advection equation, Eq. (3), for each cell in a conservative form given by

$$C_k^{n+1} - C_k^n + \Delta t \sum_f C_{k,f}^n \underline{u}_f \cdot \underline{n}_f A_f = 0, \quad (9)$$

where $C_{k,f}$ is evaluated by a first-order upwind plus flux limiter (FUDFL) convective numerical scheme [20].

The solution of the discretizated volume fraction equation, Eq. (9), provides a non-uniform thickness interface due to numerical diffusion. Hence, an artificial compression of the interface is applied, in order to mantain the profile and thickness of the interface constant, by solving to steady state the reinitialization equation

$$\frac{\partial C_k}{\partial \tau} + \nabla \cdot C_k(1 - C_k)\underline{n} = \varepsilon \nabla \cdot \nabla C_k, \quad (10)$$

where $\underline{n} = \frac{\nabla C_k}{||\nabla C_k||^2}$, $C_k(1 - C_k)\underline{n}$ is a compressive flux evaluated by a central difference (CD) convective numerical scheme [21], τ is the reinitialization time and $\varepsilon \nabla \cdot \nabla C_k$ is an artificial diffusion term added to avoid discontinuities.

3.2. Multiphase momentum equation

Multiphase flows present high discontinuities in the domain due to the density difference between fluids. Therefore, in order to avoid possible spurious pressure modes, the momentum equation is discretizated following the unstructured staggered formulation by Perot [17]. This mesh scheme, instead of evaluating velocities at cell centers, evolves normal face velocities, $u = \underline{u} \cdot \underline{n}_f$, in time. The velocity-pressure coupling is solved by using a fractional step procedure [22] written as

$$\underline{u}^{n+1} - \underline{u}^* = -\frac{\Delta t}{\rho^{n+1}} \nabla p^{n+1}. \quad (11)$$

The predictor normal face velocity, $u^* = \underline{u}^* \cdot \underline{n}_f$, is evaluated for each face from

$$T + C = D + F, \quad (12)$$

$$T \equiv \frac{\rho_f^{n+1} u^* - \rho_f^n u^n}{\Delta t} W^f A_f,$$
$$C \equiv \underline{n}_f \cdot (W_{c_1}^f \underline{C}_{c_1}^n + W_{c_2}^f \underline{C}_{c_2}^n) A_f,$$
$$D \equiv \underline{n}_f \cdot (W_{c_1}^f \underline{D}_{c_1}^n + W_{c_2}^f \underline{D}_{c_2}^n) A_f,$$
$$F \equiv \underline{n}_f \cdot (W_{c_1}^f \underline{F}_{c_1}^n + W_{c_2}^f \underline{F}_{c_2}^n) A_f,$$

where geometric parameters are shown in Fig. 1, *T*, *C*, *D* and *F* stand for transient, convective, incompressible diffusive and body force cell-centered terms defined as

$$\underline{C}_c = \frac{1}{V_c} \sum_f \dot{m}_f \underline{u}_f, \tag{13}$$

$$\underline{D}_c = \frac{1}{V_c} \sum_f \mu_f \frac{\underline{u}_F - \underline{u}_P}{W^f} A_f, \tag{14}$$

$$\underline{F}_c = \rho_c \underline{g}, \tag{15}$$

and $\underline{u}_f$ is the convected face velocity evaluated by an upwind convective numerical scheme.

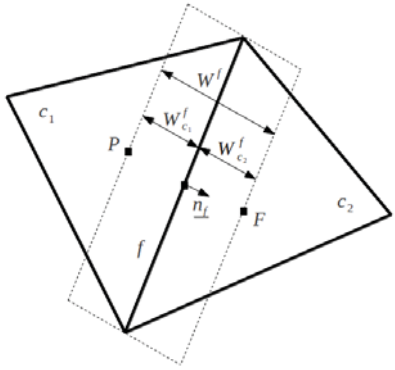

Figure 1. Notation for the unstructured staggered mesh scheme on a 2D unstructured mesh.

The pressure Poisson's equation, applying the divergence operator on both sides of Eq. 11, results in

$$\sum_f \hat{u}^* A_f = \frac{\Delta t}{\rho^{n+1}} \sum_f \frac{p_F^{n+1} - p_P^{n+1}}{W^f} A_f, \tag{16}$$

which is solved by a preconditioned conjugate gradient solver [23] giving the new pressure field. Then, new normal face velocity equals

$$u^{n+1} - u^* = -\frac{\Delta t}{\rho_f^{n+1}} \frac{p_F^{n+1} - p_P^{n+1}}{W^f}. \tag{17}$$

Finally, new cell centered velocity is interpolated from normal face velocities as

$$\underline{u}_c^{n+1} = \frac{1}{V_c} \sum_f (\underline{x}_f^{CG} - \underline{x}_c^{CC}) \hat{u}^{n+1} A_f. \tag{18}$$

4. RM INSTABILITY RESULTS

The instability simulations are based on the 2D and 3D experiments of Niederhaus and Jacobs [3] and Chapman and Jacobs [4], respectively. The 2D tank is 119.9 mm in width and 254.4 mm in height, on the other hand, the dimensions for the 3D case are 72.6 mm in width and depth and 250 mm in height. The lighter upper fluid and the heavier bottom fluid result in an Atwood number equal to $A = (\rho_2 - \rho_1)/(\rho_2 + \rho_1) = 0.1587$. At the beginning of the calculations a small periodical disturbance of the surface shape with 2D amplitude $a_0 = 0.23/k$ and wavelength $\lambda = 82.6$, and 3D amplitude $a_0 = 0.38/k$ and wavelength $\lambda = 48.4$, where $k = 2\pi/\lambda$, are incorporated to make the system unstable. Then, the initial disturbances are approximated as 2D $\eta = a_0 \cdot \sin(kx)$ and 3D $\eta = a_0[sin(kx) + sin(ky)]$. The experimental acceleration pulse imparted to the fluids is approximated as a triangular shape with a duration of 26 ms, a peak magnitude of 50g, and an integrated impulse ΔV of 6.4 m/s.

Variables used to compare numerical results to experimental ones are defined in Fig. 2. Where a, a_b and a_s stand for total, bubble and spike amplitudes and $\dot{a}$, $\dot{a}_b$ and $\dot{a}_s$ represent total, bubble and spike velocities.

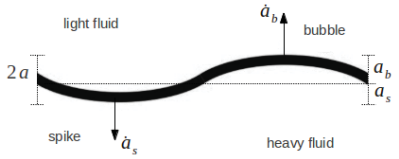

Figure 2. Schematics of the interface variables used to analyze the RM instability.

The two interface tracking methods previously presented, VOF and LS, are used to solve the instability and results are compared to experimental ones. The 2D and 3D cases are numerically solved using cartesian and unstructured meshes with average grid size of 0.0025; i.e. 4900 cells (2D test) and 84000 cells (3D test). A fixed time step of $5.0e^{-4}$ seconds is used to evolve discretized equations in time. The numerical conservation of kth fluid volume in relative value, defined as the amount of volume lost or gained respect to the initial one divided by the initial one, is approximately $1.0e^{-6}$ and $1.0e^{-4}$ when using VOF and LS in unstructured meshes, respectively.

Figures 3 and 4 are a sequence of images showing the evolution of the 2D and 3D instabilities using the two interface tracking methods, and compared to the Planar Laser-Induced Fluorescence (PLIF) images from experiments. The impulsive acceleration in these experiments is directed from the heavier fluid into the lighter one. Thus, the observed amplitude changes sign before growing. Immediately after inversion, the instability retains a sinusoidal shape. Though, with time, vortices begin to form producing the typical mushroom pattern of the RM instability.

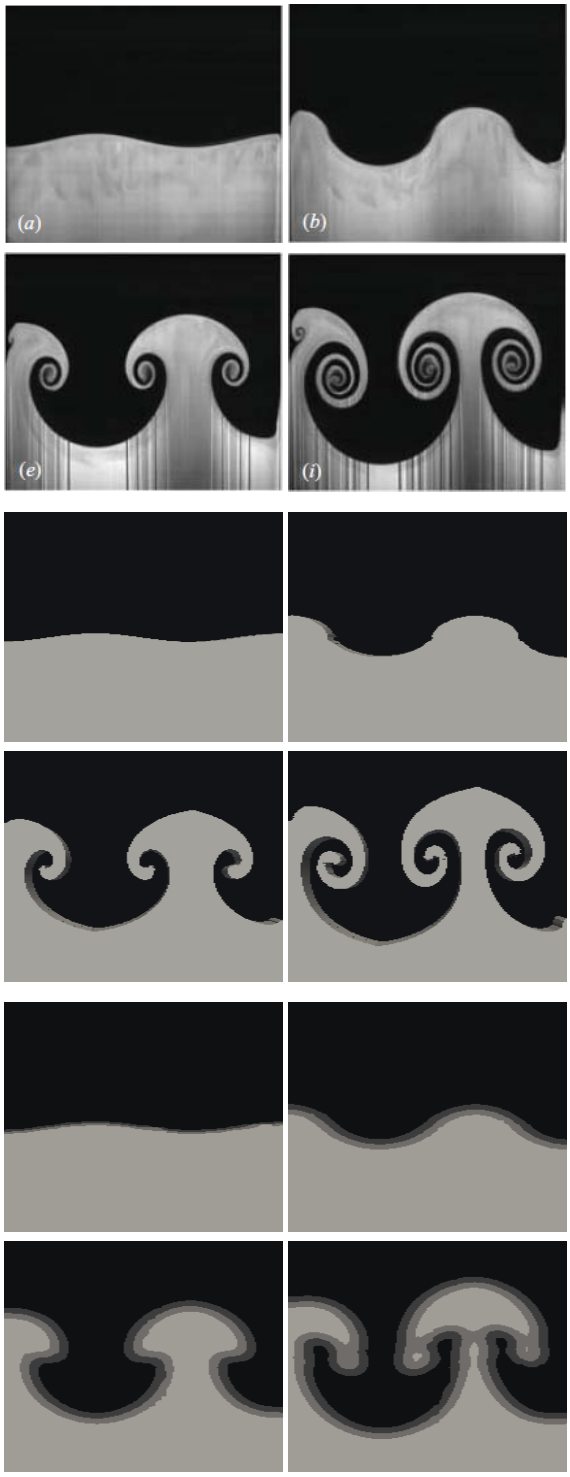

Figure 3. Three blocks of images showing the bottom fluid of the 2D RM instability tests.

Figure 3 contains three blocks of images showing the bottom fluid in the 2D RM instability tests. Blocks: (top) PLIF images from the Niederhaus and Jacobs [3] experiment, (center) interface reconstruction planes using cartesian mesh and VOF method and (bottom) volume fraction contours using cartesian mesh and LS method. Times are: (first) -14 ms, (second) 102 ms, (third) 353 ms and (fourth) 686 ms.

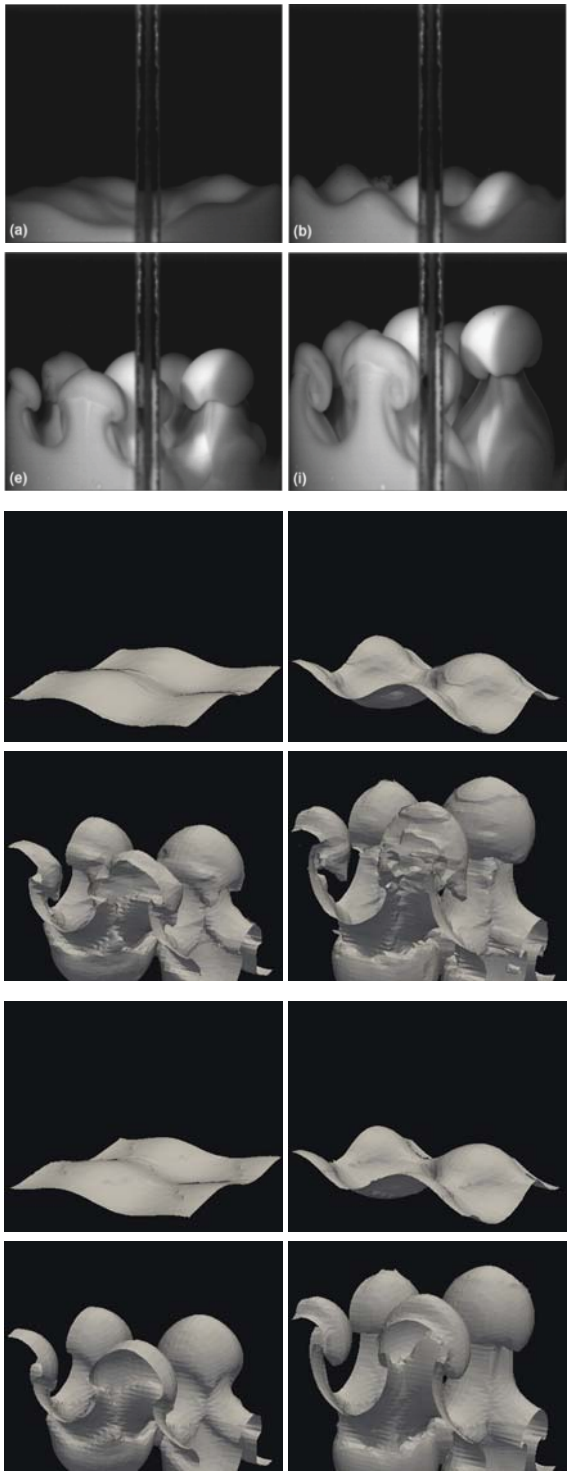

Figure 4. Three blocks of images showing the bottom fluid of the 3D RM instability tests.

Three blocks of images representing the bottom fluid in the 3D RM instability tests are shown in Figure 4. Blocks: (top) PLIF images from the Chapman and Jacobs [4] experiment, (center) 0.5 volume fraction contour using unstructured mesh and VOF and (bottom) 0.5 volume fraction contour using unstructured mesh and LS. Times are: (first) -33 ms, (second) 50 ms, (third) 300 ms and (fourth) 633 ms.

4.1. Amplitude measurements

Figures 5 and 6 show the 2D and 3D RM instability's amplitude along time for experimental and numerical results. These amplitude measurements are made dimensionless as done in the experiments of Niederhaus, Chapman and Jacobs [3, 4], by scaling amplitude with wave number k and time with wave number and theoretical initial growth rate $\dot{a}_0$.

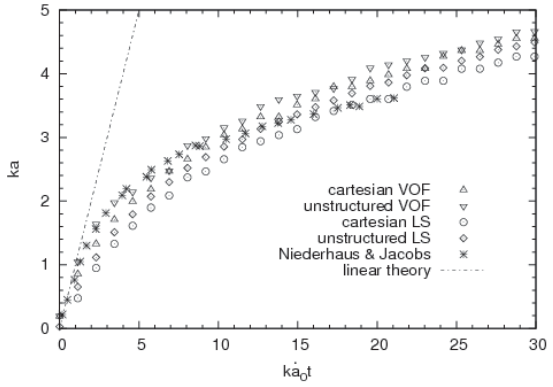

Figure 5. Plot of nondimensional amplitude versus nondimensional time for the 2D tests.

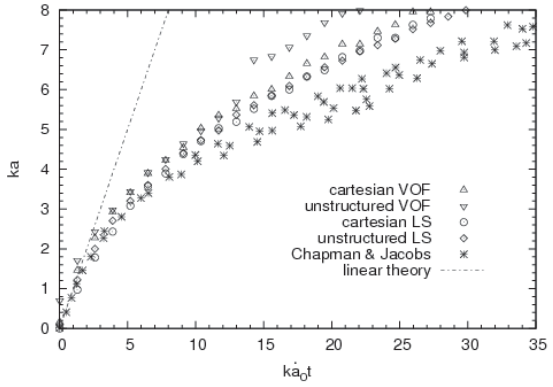

Figure 6. Plot of nondimensional amplitude versus nondimensional time for the 3D tests.

The linear theory that describes the early stages of the RM instability, developed by Richtmyer [1], is shown to be satisfied until nondimensional time 2 - 3 both by experimental results and numerical solutions from the interface tracking methods and mesh configurations used in this work. On the other hand, numerical results of the late time instability's amplitude follow the pattern of experimental ones but they are not accurate enough, though, it is believed that numerical results would merge with experimental ones if meshes are densified.

4.2. Velocity measurements

The velocity, defined as the average of bubble and spike velocities, for the 2D and 3D RM instability's experimental and numerical results is plotted along time in Figures 7 and 8. The velocity is non-dimensionalized dividing by theoretical initial growth rate $\dot{a}_0$.

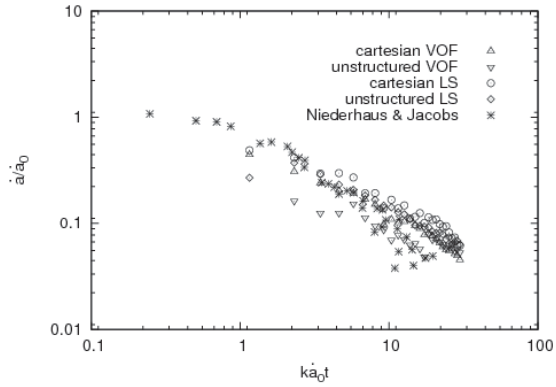

Figure 7. Plot of nondimensional velocity versus nondimensional time for the 2D tests

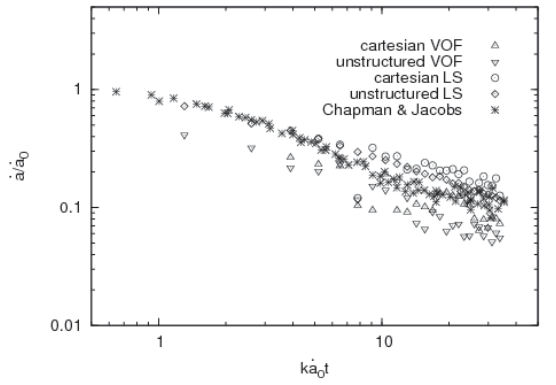

Figure 8. Plot of nondimensional velocity versus nondimensional time for the 3D tests.

It is observed, from experimental and numerical results, that 3D velocities present slightly faster nonlinear growth than the 2D ones. This 2D - 3D difference in velocity behaviour is due to the configurations of the vorticity fields: 2D vortexs are stationary while 3D vortex rings move alternately upward and downward as it is shown in Figures 9 and 10. As a result, 2D interface velocity decays with time as it is pushed away from the vortex centers. On the other hand, in the 3D flow the interface velocity is the sum of a decaying component similar to the 2D flow and the vortex ring velocity associated to the vortex stretching mechanism. Thus, with time, interface velocity approaches the vortex ring one.

4.3. Vorticity

The vorticity equation, simplified for incompressible flows of inviscid fluids and conservative body forces, is written as

$$\frac{D\underline{\omega}}{Dt} = (\underline{\omega} \cdot \nabla)\underline{u} + \frac{1}{\rho^2}\nabla\rho \times \nabla p, \tag{19}$$

where vorticity is defined as $\underline{\omega} = \nabla \times \underline{u}$, the term on the left-hand side is the material derivative of the vorticity

vector that describes the rate of change of angular acceleration of the fluid, first term on the right-hand side describes the stretching or tilting of vorticity due to velocity gradients and the second term is the baroclinic mechanism which accounts for changes in vorticity due to intersectioning of density and pressure isosurfaces.

In the RM instabilities studied in this work, vorticity is created during the impulsive acceleration by the baroclinic term of Eq. 19. In detail, the pressure gradient during the impulsive acceleration is hydrostatic and thus oriented in the direction of the acceleration while the density gradient is perpendicular to the fluid interface. In the 2D instability case the distribution of these gradients result in the formation of vortices oriented perpendicular to the viewing plane, which are shown in Fig. 9. The 3D case, however, results in the vorticity distribution of Fig. 10, which consists of an array of vortex rings.

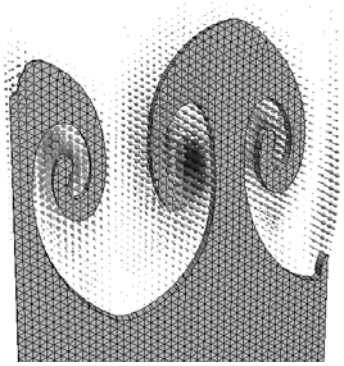

Figure 9. Vorticity vectors, VOF planes and mesh of the 2D RM instability test.

The difference between 2D and 3D velocity behaviour due to the vortex stretching mechanism, stated in Section 4.2, is explained by calculating the first term on the right-hand side of Eq. 19 using Figures 9 and 10. The 2D case results in a null vector space, since $\underline{\omega} = (0, 0, \omega_z)$ and the zth derivatives of the velocity tensor are equal to zero. However, the 3D case presents two main vectors with opposite senses at the crests of the bubbles and spikes, meaning that the interface of the instability is being stretched and its amplitude increased by the vortex stretching mechanism.

5. CONCLUSIONS

In this work an assesment of two different 3D interface tracking algorithms has been done. The VOF and LS interface tracking methods for 3D general meshes have been shown to correctly calculate the evolution of 2D and 3D RM instabilities initiated with single-mode perturbations. Hence, CFD for multiphase flow is proven to be an excellent tool to study RM instabilities. In particular, the self-developed interface tracking methods for 3D unstructured meshes present good results, encouraging the authors to test them against more industry oriented multiphase problems.

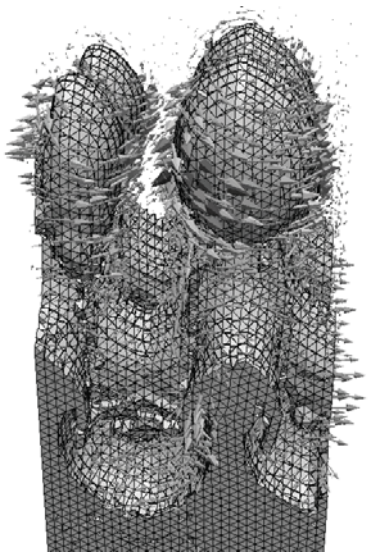

Figure 10. Vorticity vectors, VOF planes and mesh of the 3D RM instability test.

The two interface tracking methods present good overall results in cartesian and unstructured meshes, see Figures 3 and 4. In particular, numerical evolution in time of interface amplitude and velocity correspond to the experimental physical behavior, shown from Fig. 5 to 8. Results using the VOF method present better detail accuracy, specifically at vortex tips, but require large computational resources, while results from LS are able to accurately calculate the main pattern of the flow in a fast way.

Analysis of the vorticity distributions, applying the vorticity equation to the results obtained from the solution of the 2D and 3D RM instabilities, reveal a main physical difference between 2D and 3D cases. In the 2D case, the stretching term of the vorticity equation due to velocity gradients is zero, while in the 3D case, the term presents two main vectors with opposite senses at the crests of bubbles and spikes. As a result, the 2D interface velocity decays with time as it is pushed away from the vortex centers, however, in the 3D flow the interface velocity approaches that of the vortex ring associated to the vortex stretching mechanism.

ACKNOWLEDGEMENTS

This work has been financially supported by the Ministerio de Ciencia e Innovación, Spain (ENE-2010-17801), a FPU grant by the Ministerio de Educación, Spain (AP-2008-03843) and by Termo Fluids S.L.

The authors would like to acknowledge sincerely Jeffrey W. Jacobs, Journal of Fluid Mechanics and Physics of Fluids for their permission to partially reproduce some images, specifically the PLIF images of the 2D and 3D RM instability in Figures 3 and 4.

References

[1] Richtmyer, R.D., 1960, "Taylor Instability in Shock Acceleration of Compressible Fluids", *Communications on Pure and Applied Mathematics*, Vol. 13(2), pp. 297-319.

[2] Meshkov, E.E., 1969, "Instability of the Interface of Two Gases Accelerated by a Shock Wave", *Izv. Ross. Akad. Nauk, Mekh. Zhidk. Gaza*, Vol. 4(5), pp. 101-104.

[3] Niederhaus, C.E. and Jacobs, J.W., 2003, "Experimental Study of the Richtmyer-Meshkov Instability of Incompressible Fluids", *Journal of Fluid Mechanics*, Vol. 485, pp. 243-277.

[4] Chapman, P. R. and Jacobs, J. W., 2006, "Experiments on the Three-Dimensional Incompressible Richtmyer-Meshkov Instability", *Physics of Fluids*, Vol. 18(7).

[5] Zhang, Q. and Sohn, S., 1999, "Quantitative Theory of Richtmyer-Meshkov Instability in Three Dimensions", *ZAMP*, VOl. 50(1).

[6] Oron, D., Arazi, L., Kartoon, D., Rikanati, A., Alon, U. and Shvarts, D., 2001, "Dimensionality Dependence of the Rayleigh-Taylor and Richtmyer-Meshkov Instability Late-Time Scaling Laws", *Physics of Plasmas*, Vol. 8(6), pp. 2883-2890.

[7] Goncharov, V. N., 2002, "Analytical Model of Nonlinear, Single-Mode, Classical Rayleigh-Taylor Instability at Arbitrary Atwood Numbers", *Phys. Rev. Lett.*, Vol. 88(13), pp. 134502-134506.

[8] Scardovelli, R. and Zaleski, S., 1999, "Direct Numerical Simulation of Free-Surface and Interfacial Flow", *Annual Review of Fluid Mechanics*, Vol. 31(-), pp. 567-603.

[9] Hirt, C. W. and Nichols, B. D., 1981, "Volume of fluid (VOF) Method for the Dynamics of Free Boundaries", *Journal of Computational Physics*, Vol. 39(5), pp. 201-225.

[10] Liovic, P., Rudman, M., Liow, J.L., Lakehal, D. and Kothe, D., 2006, "A 3D Unsplit-Advection Volume Tracking Algorithm with Planarity-Preserving Interface Reconstruction", *Computers and Fluids*, Vol. 35(10), pp. 1011-1032.

[11] Jofre, L., Lehmkuhl, O., Castro, J. and Oliva A., 2010, "A PLIC-VOF Implementation on Parallel 3D Unstructured Meshes", Proc. *Fifth European Conference on Computational Fluid Dynamics*, pp. 1-15.

[12] Osher, S. and Sethian, J., 1988, "Fronts Propagating with Curvature Dependent Speed: Algorithms Based on Hamilton-Jacobi Formulations", *Journal of Computational Physics*, Vol. 79, pp. 12-49.

[13] Olsson, E. and Kreiss, G., 2005, "A conservative Level Set method for two phase Flow", *Journal Computational Physics*, Vol. 210, pp. 225-246.

[14] Rhie, C.M. and Chow, W.L., 1983, "Numerical Study of th Turbulent Flow Past an Airfol with Trailing Edge Separation", *AIAA Journal*, Vol. 21, pp. 1525-1532.

[15] Mahesh, K., Constantinescu, G. and Moin, P., 2004, "A Numerical Method for Large-Eddy Simulation in Complex Geometries", *Journal of Computational Physics*, Vol. 197, pp. 215-240.

[16] Lehmkuhl, O., Borrell, R., Pérez-Segarra, C.D. and Oliva, A., 2009, "Direct numerical simulations and symmetry-preserving regularization simulations of the flow over a circular cylinder at Reynolds number 3900", Proc *VI International Symposium on Turbulence, Heat and Mass Transfer*, pp. 325-328.

[17] Perot, B., 2000, "Conservation Properties of Unstructured Staggered Mesh Schemes", *Journal of Computational Physics*, Vol. 159, pp. 58-89.

[18] Harlow, F. H. and Welch, J. E., 1965, "Numerical Calculation of Time-Dependent Viscous Incompressible Flow of Fluid with Free Surface", *Physics of Fluids*, Vol. 8(12), pp. 2182-2189.

[19] Youngs, D.L., 1982, "Time-Dependent Multi-Material Flow with Large Fluid Distortion", Proc *Numerical Methods for Fluid Dynamics Conference*, pp. 273-285.

[20] Sweby, P.K., 1984, "High Resolution Schemes using Flux Limiters for Hyperbolic Conservation Laws", *SIAM Journal of Numerical Analysis*, Vol. 21(5), pp. 995-1011.

[21] Yeoh, G.H. and Tu, J., 2009, *Computational Techniques for Multiphase Flows*, Elsevier Science Publishing Co. Inc.

[22] Chorin, A.J., 1968, "Numerical Solution of the Navier-Stokes Equations", *Journal of Computational Physics*, Vol. 22, pp. 745-762.

[23] Shewchu,k J.R., 1994, "An Introduction to the Conjugate Gradient Method without the Agonizing Pain", *Technical Report* Carnegie Mellon University.